The Reflection Definition of the Characteristic Impedance of Microstrips

FRITZ ARNDT AND G. U. PAUL

Abstract—**The frequency-dependent characteristic impedance of shielded microstrips is computed by the scattering matrix of the step of a rectangular transmission line to the shielded microstrip including higher order hybrid modes. This method avoids the ambiguities of the hitherto known definitions based on TEM quantities. For the dispersion characteristics a resonant model is used which reduces the number of the characteristic equations required. Numerical results are given including strips of finite thickness placed unsymmetrically in the shielded microstrip.**

I. Introduction

BIANCO *et al.* [1] discuss the hitherto known definitions of the characteristic impedance of microstrips. Denlinger's TEM-like expression [2] leads to a decreasing function. The other definitions [3]–[8] lead to an increasing function. Although there exist hybrid-mode solutions for the propagation constant of microstrip lines, the definitions for their characteristic impedance are still based amazingly on TEM quantities like "mean voltage" or "total current" which lose their uniqueness since other than TEM modes propagate.

The purpose of this paper is to present a hybrid-mode concept for calculating the frequency-dependent characteristic impedance of shielded microstrip lines which may help to resolve the obvious discrepancy between the known definitions. Hereto, the scattering matrix of the step of the rectangular transmission line with its known characteristic impedance [9], [10] to the shielded microstrip line (Fig. 1) is computed including higher order hybrid modes. Using the relation between the reflection coefficient and the related input impedance [11], [12] the interesting frequency-dependent characteristic impedance can then be determined within an accuracy which depends on the number of the hybrid modes considered. This definition is adequate for the microstrip wave-propagation concept since it takes into account the hybrid-mode solution, and avoids the above-mentioned ambiguities.

Concerning the eigenfunctions of the shielded microstrip line necessary for the field matching at the step investigated (Fig. 1) for finite thick strips, it is appropriate to use a method different from that given in [13], where a subdivision into eight partial waveguides is required. The cross section of the shielded microstrip line can be interpreted as a line resonator. This reduces the number of characteristic equations required and thus allows more hybrid modes to be considered. As a secondary objective of this paper the dispersion characteristics of the first eight hybrid modes are computed by this method and compared with some results presented in [13], [14]. Further, the analysis given holds for finite, thick strips placed unsymmetrically in the shielded microstrip line.

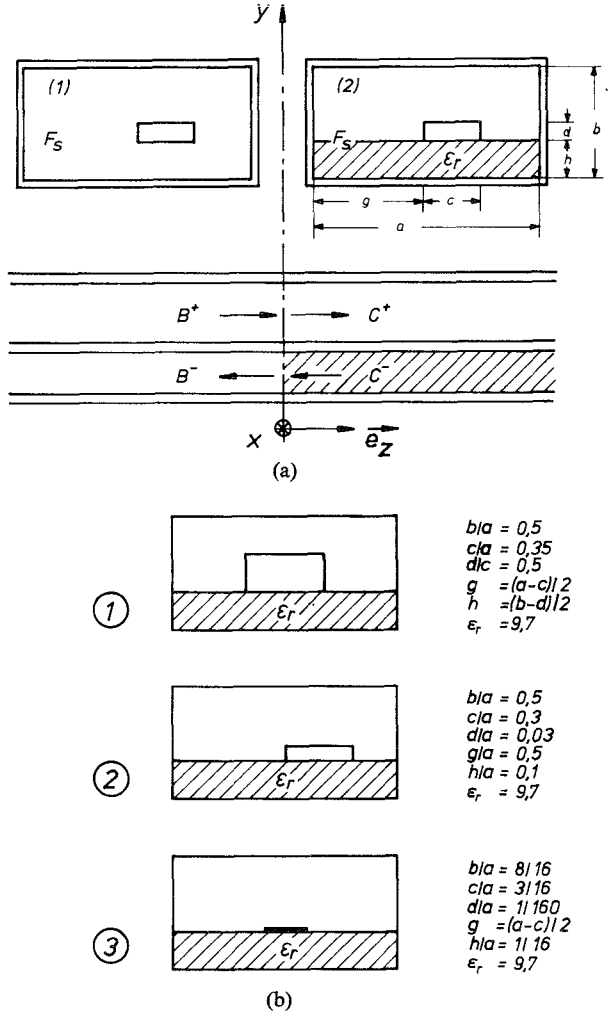

Fig. 1. Investigated microstrip transmission lines. (a) Step between a homogeneous- and an inhomogeneous-filled shielded stripline. (b) Investigated cross section types.

Manuscript received July 24, 1978; revised December 8, 1978.

F. Arndt is with the Department of Microwaves, University of Bremen, D-2800 Bremen, Germany.

G. U. Paul was with the Department of Microwaves, University of Bremen, Germany. He is now with the Central Development Department, Brown, Boverie and Cie, D-6800 Mannheim, Germany.

0018-9480/79/0800-0724$00.75 ©1979 IEEE

II. Formulation of the Method

A. Eigenfunctions for the Shielded Microstrip Line

The hybrid modes on the shielded microstrip line are derived from the axial z-components of the vector potentials A_h and A_e:

$$E = \text{rot}\,(A_{hz}\vec{e}_z) + \frac{1}{j\omega\epsilon}\,\text{rot rot}\,(A_{ez}\vec{e}_z)$$

$$H = -\frac{1}{j\omega\mu}\,\text{rot rot}\,(A_{hz}\vec{e}_z) + \text{rot}\,(A_{ez}\vec{e}_z). \tag{1}$$

The subdivision of the cross section according to Fig. 2(a) leads to four parallel plate lines. Their vector potentials can be written as a product of the eigenfunctions $V_{h,e}(x,y)$ with the common propagation expression $e^{-jk_z z}$ and the square roots[1] of the field impedances

$$Z_h = 1/Y_h = \frac{\omega\mu}{k_z} \qquad Z_e = 1/Y_e = \frac{k_z}{\omega\epsilon} \tag{2}$$

$$A_{hz} = \sqrt{Z_h^\nu}\; V_h^\nu(x,y)e^{-jk_z z}$$

$$A_{ez} = \sqrt{Y_e^\nu}\; V_e^\nu(x,y)e^{-jk_z z}$$

$$\nu = \text{I, II}a\text{, II}b\text{, and III} \tag{3}$$

with

$$V_h^{\text{I}} = \sum_{n=0}^{\infty} \frac{\cos\dfrac{n\pi x}{a}}{\sqrt{1+\delta_{on}}}\left[A_n^{\text{I}}e^{+jk_{yn}^{\text{I}}y} + B_n^{\text{I}}e^{-jk_{yn}^{\text{I}}y}\right]$$

$$V_h^{\text{II}a} = \sum_{n=0}^{\infty} \frac{\cos\dfrac{n\pi x}{g}}{\sqrt{1+\delta_{on}}}\left[A_n^{\text{II}a}e^{+jk_{yn}^{\text{II}a}y} + B_n^{\text{II}a}e^{-jk_{yn}^{\text{II}a}y}\right]$$

$$V_h^{\text{II}b} = \sum_{n=0}^{\infty} \frac{\cos\dfrac{n\pi(x-g-c)}{a-g-c}}{\sqrt{1+\delta_{on}}}\left[A_n^{\text{II}b}e^{+jk_{yn}^{\text{II}b}y} + B_n^{\text{II}b}e^{-jk_{yn}^{\text{II}b}y}\right]$$

$$V_h^{\text{III}} = \sum_{n=0}^{\infty} \frac{\cos\dfrac{n\pi x}{a}}{\sqrt{1+\delta_{on}}}\left[A_n^{\text{III}}e^{+jk_{yn}^{\text{III}}y} + B_n^{\text{III}}e^{-jk_{yn}^{\text{III}}y}\right] \tag{4}$$

$$V_e^{\text{I}} = \sum_{n=1}^{\infty} \sin\frac{n\pi x}{a}\,\frac{1}{jk_{yn}^{\text{I}}}\left[C_n^{\text{I}}e^{+jk_{yn}^{\text{I}}y} - D_n^{\text{I}}e^{-jk_{yn}^{\text{I}}y}\right]$$

$$V_e^{\text{II}a} = \sum_{n=1}^{\infty} \sin\frac{n\pi x}{g}\,\frac{1}{jk_{yn}^{\text{II}a}}\left[C_n^{\text{II}a}e^{+jk_{yn}^{\text{II}a}y} - D_n^{\text{II}a}e^{-jk_{yn}^{\text{II}a}y}\right]$$

$$V_e^{\text{II}b} = \sum_{n=1}^{\infty} \sin\frac{n\pi(x-g-c)}{a-g-c}\,\frac{1}{jk_{yn}^{\text{II}b}} \cdot\left[C_n^{\text{II}b}e^{+jk_{yn}^{\text{II}b}y} - D_n^{\text{II}b}e^{-jk_{yn}^{\text{II}b}y}\right]$$

[1]The amplitudes of the waves are so normalized that the transported power

$$P = \int_{F_s} E\times H^* dF = \sqrt{Z}\,\sqrt{Y}^* \int_{F_s} (\text{grad}\,V\times\vec{e}_z\times\text{grad}\,V)\cdot\vec{e}_z dF$$

is 1 W for an amplitude 1 V/cm or 1 A/cm, respectively. The factor $\sqrt{Z}\,\sqrt{Y^*}$ leads to 1 for $k_z^2>0$, and to $\pm j$ for $k_z^2<0$.

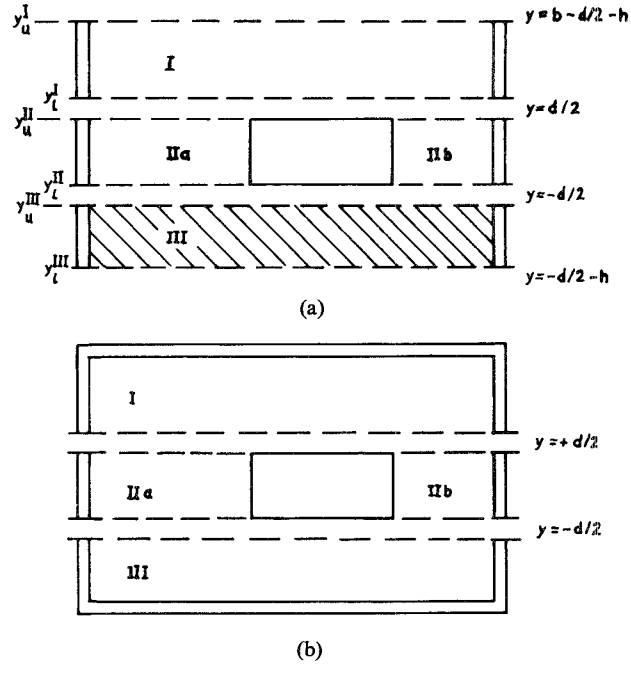

Fig. 2. Subdivision of the cross sections. (a) Subdivision of the cross section of the shielded microstrip line into four parallel plate lines (the boundary conditions at $y = b - d/2 - h$ and $y = -d/2 - h$ are satisfied by the resonant condition (11).) (b) Rectangular transmission line (homogeneous shielded stripline).

$$V_e^{\text{III}} = \sum_{n=1}^{\infty} \sin\frac{n\pi x}{a}\,\frac{1}{jk_{yn}^{\text{III}}}\left[C_n^{\text{III}}e^{+jk_{yn}^{\text{III}}y} - D_n^{\text{III}}e^{-jk_{yn}^{\text{III}}y}\right] \tag{5}$$

δ_{on} = Kronecker delta.

B. Dispersion Characteristics of the Hybrid Modes

The eigenfunctions $V(x,y)$ can be regarded as representing waves traveling in the $\pm y$ direction, with the still unknown propagation constant k_y. It is possible to define the amplitudes:

$$I_{hn}^\nu(y) = A_n^\nu e^{+jk_{yn}^\nu y} + B_n^\nu e^{-jk_{yn}^\nu y}$$

$$U_{hn}^\nu(y) = \frac{dI_{hn}^\nu}{dy} = jk_{yn}^\nu[A_n^\nu e^{+jk_{yn}^\nu y} - B_n^\nu e^{-jk_{yn}^\nu y}]$$

$$U_{en}^\nu(y) = \frac{1}{jk_{yn}^\nu}[C_n^\nu e^{+jk_{yn}^\nu y} - D_n^\nu e^{-jk_{yn}^\nu y}]$$

$$I_{en}^\nu(y) = \frac{dU_{en}^\nu}{dy} = C_n^\nu c^{+jk_{yn}^\nu y} + D_n^\nu e^{-jk_{yn}^\nu y}. \tag{6}$$

The sum of the amplitudes of the waves in each parallel plate line υ (Fig. 2(a)) at its lower boundary ($y = y_l^\upsilon$) is determined by the sum of the amplitudes at its upper boundary ($y = y_u^\upsilon$):

$$\begin{bmatrix} U_h^\nu \\ U_e^\nu \\ I_h^\nu \\ I_e^\nu \end{bmatrix}_{y=y_l^\nu} = \begin{bmatrix} L_{s'}^\nu & 0 & L_{c'}^\nu & 0 \\ 0 & L_c^\nu & 0 & L_s^\nu \\ L_s^\nu & 0 & L_c^\nu & 0 \\ 0 & L_{c'}^\nu & 0 & L_{s'}^\nu \end{bmatrix} \begin{bmatrix} U_h^\nu \\ U_e^\nu \\ I_h^\nu \\ I_e^\nu \end{bmatrix}_{y=y_u^\nu} \tag{7}$$

with the diagonal matrices

$$(L_c^\nu)_{nn} = \cos(k_{yn}^\nu w) \qquad (L_{c'}^\nu) = -k_{yn}^\nu \sin(k_{yn}^\nu w)$$

$$(L_s^\nu)_{nn} = \frac{1}{k_{yn}^\nu}\sin(k_{yn}^\nu w) \qquad (L_{s'}^\nu) = \cos(k_{yn}^\nu w)$$

$$w = y_l^\nu - y_u^\nu. \tag{8}$$

The indexes c and s denote the cosine and sine function (for $k_{yn}^{\nu 2} \leqslant 0$ the corresponding hyperbolic functions must be chosen.)

The boundary conditions at the partial waveguides

$$0<x<g \quad : E_{x,z}^{\mathrm{III}} = E_{x,z}^{\mathrm{II}a} \qquad H_{x,z}^{\mathrm{III}} = H_{x,z}^{\mathrm{II}a}$$

$$g<x<g+c: E_{x,z}^{\mathrm{III}} = 0$$

$$g+c<x<a \quad : E_{x,z}^{\mathrm{III}} = E_{x,z}^{\mathrm{II}b} \qquad H_{x,z}^{\mathrm{III}} = H_{x,z}^{\mathrm{II}b} \tag{9}$$

successively applied to (7) lead finally to the relation between the amplitudes at the lower boundary ($y = y_l^{\mathrm{III}} = -d/2-h$) and the amplitudes at the upper boundary ($y = y_u^{\mathrm{I}} = b-d/2-h$, Fig. 2(a)):

$$\begin{bmatrix} U_h^{\mathrm{III}} \\ U_e^{\mathrm{III}} \\ I_h^{\mathrm{III}} \\ I_e^{\mathrm{III}} \end{bmatrix} = L^{\mathrm{III}} K_{\mathrm{III}}^{\mathrm{II}} L^{\mathrm{II}} K_{\mathrm{II}}^{\mathrm{I}} L^{\mathrm{I}} \begin{bmatrix} U_h^{\mathrm{I}} \\ U_e^{\mathrm{I}} \\ I_h^{\mathrm{I}} \\ I_e^{\mathrm{I}} \end{bmatrix} \tag{10}$$

$$y = y_l^{\mathrm{III}} \qquad\qquad y = y_u^{\mathrm{I}}.$$

The quasi-transmission-line matrices L^υ (υ=I, II, III) (cf. (8)) transform the amplitudes from the upper to the lower boundary. The transition matrices $K_{\mathrm{III}}^{\mathrm{II}}$ and $K_{\mathrm{II}}^{\mathrm{I}}$ (cf. Appendix) transform the amplitudes between the adjacent parallel plate lines.

The still missing boundary condition at the metallic surfaces at $y = -d/2-h$ and $y = b-d/2-h$ leads to the resonant condition:

$$O = \begin{bmatrix} M_{hh} & M_{he} \\ M_{eh} & M_{ee} \end{bmatrix} \begin{bmatrix} I_h^{\mathrm{I}} \\ I_e^{\mathrm{I}} \end{bmatrix}. \tag{11}$$

The matrix of this characteristic equation (11) is the upper right quarter of the matrix product of (10). The zeros of the determinant which is a transcendent function of $k_{yn}(\omega, \epsilon_{\mathrm{eff}})$:

$$\left(k_{yn}^{\mathrm{I}}\right)^2 = \omega^2\mu(\epsilon_0 - \epsilon_{\mathrm{eff}}) - \left(\frac{n\pi}{a}\right)^2$$

$$\left(k_{yn}^{\mathrm{II}}\right)^2 = \omega^2\mu(\epsilon_0 - \epsilon_{\mathrm{eff}}) - \left(\frac{n\pi}{\tilde{g}}\right)^2$$

$$\left(k_{yn}^{\mathrm{III}}\right)^2 = \omega^2\mu(\epsilon_0\epsilon_r - \epsilon_{\mathrm{eff}}) - \left(\frac{n\pi}{a}\right)^2 \tag{12}$$

$$\tilde{g} = \begin{cases} g & \text{region II}a \text{ (Fig. 2}(a)\text{)} \\ a-g-c & \text{region II}b \end{cases}$$

provide the interesting dispersion characteristic.

C. Eigenfunctions for the Rectangular Transmission Line

The cross section is suitably subdivided (Fig. 2(b)). Unlike the treatment given in [9], the modes are each derived from only one vector potential corresponding to (3), and so remain uncoupled also beyond their cutoff frequency. The eigenfunctions $T(x,y)$ for the rectangular transmission line are still similar to those given in [9] and are merely stated in Appendix II for completeness.

D. The Scattering Matrix of the Step

Fig. 1 shows the step investigated. The transversal E- and H-field strengths of the adjacent transmission lines (1) and (2) are expressed by the eigenfunctions:

$$\vec{E}_t^{(1)} = \sum_j \sqrt{Z_j}\,\vec{e}_{tj}\left(B_j^+ e^{-jk_{zj}z} + B_j^- e^{+jk_{zj}z}\right)$$

$$\vec{H}_t^{(1)} = \sum_j \sqrt{Y_j}\,\vec{h}_{tj}\left(B_j^+ e^{-jk_{zj}z} - B_j^- e^{+jk_{zj}z}\right)$$

$$\vec{e}_{tj} = \begin{Bmatrix} \text{grad } T_h \times \vec{e}_z, & H\text{-mode} \\ -\text{grad } T_e, & E\text{-mode} \\ -\text{grad } T_1, & \text{TEM-mode} \end{Bmatrix}$$

$$\vec{h}_{tj} = \vec{e}_z \times \vec{e}_{tj} \tag{13}$$

$$\vec{E}_t^{(2)} = \sum_k \vec{e}_{tk}\left(C_k^+ e^{-jk_{zk}z} + C_k^- e^{+jk_{zk}z}\right)$$

$$\vec{H}_t^{(2)} = \sum_k \vec{h}_{tk}\left(C_k^+ e^{-jk_{zk}z} - C_k^- e^{+jk_{zk}z}\right)$$

$$\vec{e}_{tk} = \sqrt{Z_{hk}}\ \text{grad } V_{hk} \times \vec{e}_z - \sqrt{Z_{ek}}\ \text{grad } V_{ek}$$

$$\vec{h}_{tk} = \sqrt{Y_{hk}}\ \text{grad } V_{hk} + \sqrt{Y_{ek}}\ \text{grad } V_{ek} \times \vec{e}_z. \tag{14}$$

(The indication υ=I, II, III, Fig. 2(a) and (b), of the subdivision of the cross sections is omitted in this chapter for simplicity.) B_j^+, C_k^+ are the amplitudes of waves traveling in the $+z$-direction, B_j^-, C_k^- are the amplitudes of waves traveling in the $-z$-direction, cf. Fig. 1. The indexes j and k designate transversal field vectors $\vec{e}_{tj}$, $\vec{k}_{tj}$, $\vec{e}_{tk}$, $\vec{h}_{tk}$ which cohere with the eigenfunctions and indicate the order of their cutoff frequencies.

The boundary conditions at the step ($z=0$)

$$E_t^{(1)} = E_t^{(2)} \qquad H_t^{(1)} = H_t^{(2)} \tag{15}$$

lead to the matrix equations

$$B^+ + B^- = (\sqrt{Y})K_e(C^+ + C^-)$$

$$B^+ - B^- = (\sqrt{Z})K_h(C^+ + C^-). \tag{16}$$

The vectors B^+, B^-, C^+, and C^- contain the amplitudes of the traveling waves, the diagonal matrices $(\sqrt{Z})$ and $(\sqrt{Y})$ contain the square roots of the magnetic- or electric-field impedances Z_h or Z_e, and the magnetic- or electric-field admittances Y_h or Y_e, respectively, (cf. (2)). The electrical K_e and the magnetic coupling matrix K_h are given by the elements

$$(K_e)_{jk} = \int_{F_S} \vec{e}_{tj}\cdot\vec{e}_{tk}\,dF \qquad (K_h)_{jk} = \int_{F_S} \vec{h}_{tj}\cdot\vec{h}_{tk}\,dF. \tag{17}$$

The scattering matrix S of the step is given by eliminating

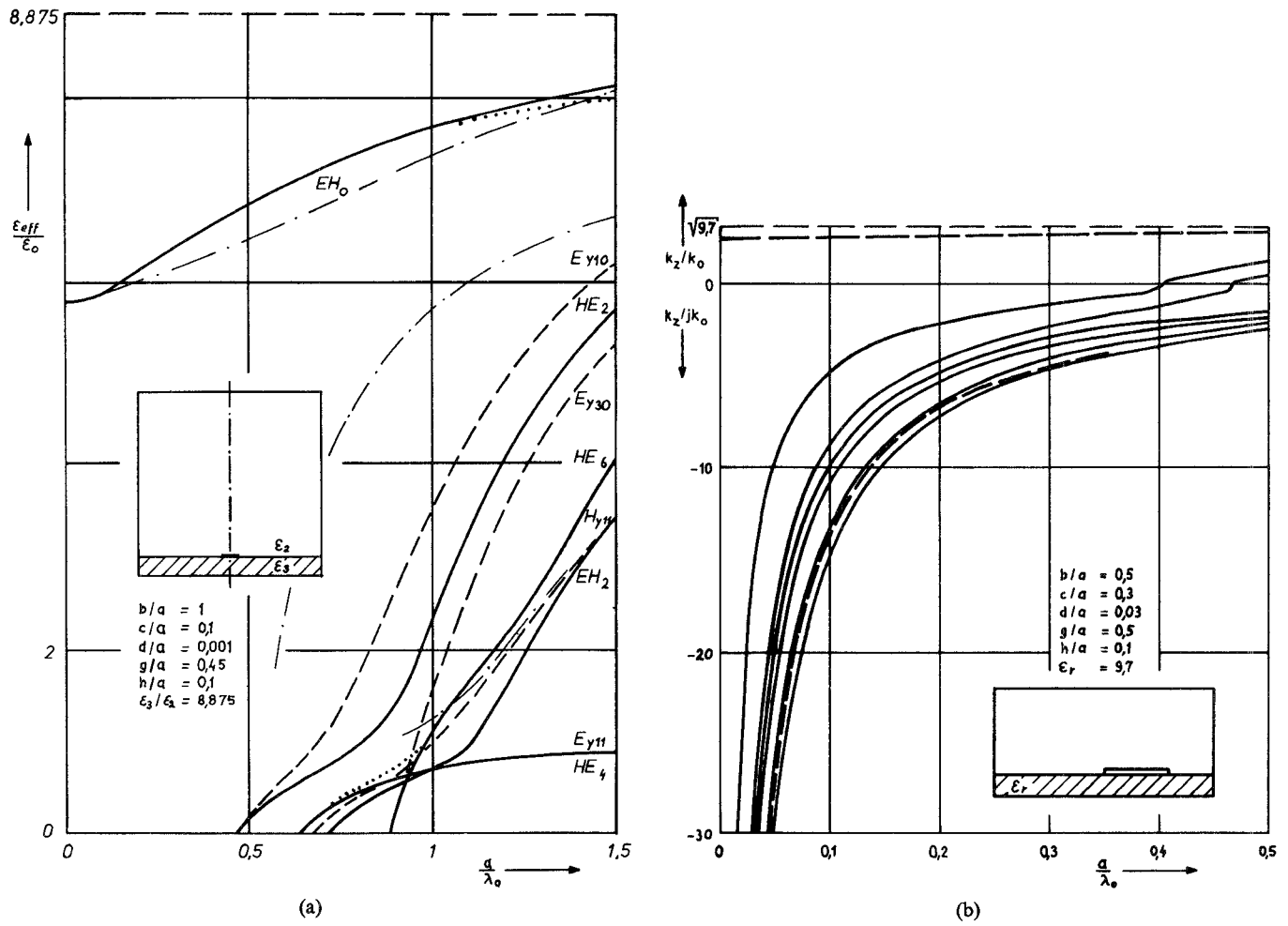

Fig. 3. Dispersion diagrams. (a) Effective dielectric constant versus a/λ_0; a = width of the shielded microstrip line (cf. Fig. 1(a); λ_0 = wavelength in air; EH_0 = hybrid mode with cutoff frequency at $f=0$ (fundamental mode); EH_2 = hybrid mode with the second cutoff frequency and a purely E-mode (TM-mode) at cutoff frequency, etc.; HE_4 = hybrid mode with the fourth cutoff frequency and a purely H-mode (TE-mode) at cutoff frequency, etc.; $E_{y10} = LSE$ mode without strip, (dotted lines ---) etc.; · · · Kowalski and Pregla [13]; -.-.- Mittra and Itoh (from graphical representation) [14]. (b) Dispersion characteristic of the first eight hybrid modes of a unsymmetrical microstrip line (cf. Fig. 1(b), ②)(——HE-modes, ---- EH-modes) k_z is the phase constant of the hybrid mode; and $k_0 = \omega\sqrt{\mu_0\epsilon_0}$.

B^- and C^+ in (16):

$$\begin{pmatrix} B^- \\ C^+ \end{pmatrix} = S \begin{pmatrix} B^+ \\ C^- \end{pmatrix} \tag{18}$$

with

$$S = \left(-\begin{pmatrix} I & 0 \\ 0 & I \end{pmatrix} + 2 \begin{pmatrix} (\sqrt{Y})K_e & 0 \\ 0 & I \end{pmatrix} \cdot \begin{pmatrix} M & M \\ M & M \end{pmatrix} \begin{pmatrix} I & 0 \\ 0 & (\sqrt{Z})K_h \end{pmatrix} \right) \tag{19}$$

and

$$M = \left((\sqrt{Y})K_e + (\sqrt{Z})K_h \right)^{-1}$$

I = unit matrix.

The characteristic impedance $Z_0(\omega)$ of the shielded microstrip line is then computed by the reflection coefficient S_{11} (19) of the TEM-mode on the rectangular transmission line [13], [14]:

$$Z_0(\omega) = Z_r \frac{1-|S_{11}|}{1+|S_{11}|} \tag{20}$$

where Z_r is the known constant characteristic impedance of the rectangular transmission line [9], [10].

III. Results

In Fig. 3(a) the dispersion characteristics of the first mode and the first higher order modes of a microstrip with a cross section according to Kowalski and Pregla [12] and Mittra and Itoh [13] are shown in order to compare the results. The dispersion curves agree largely with those of Kowalski and Pregla. They computed, however, only the first two higher order modes and did not notice that dispersion curves of hybrid modes can cross one another in contrast to those of pure E- or H-modes. Our results do not agree with Mittra and Itoh, especially the higher order modes. Fig. 3(b) shows the dispersion characteristics of the first eight eigenwaves of a unsymmetrical finite thick microstrip line.

In order to obtain an impression of the accuracy of the computations the variation of the propagation constant k_z with the number N of eigenwaves was considered. For N greater then eight, the variation of k_z was less than 1

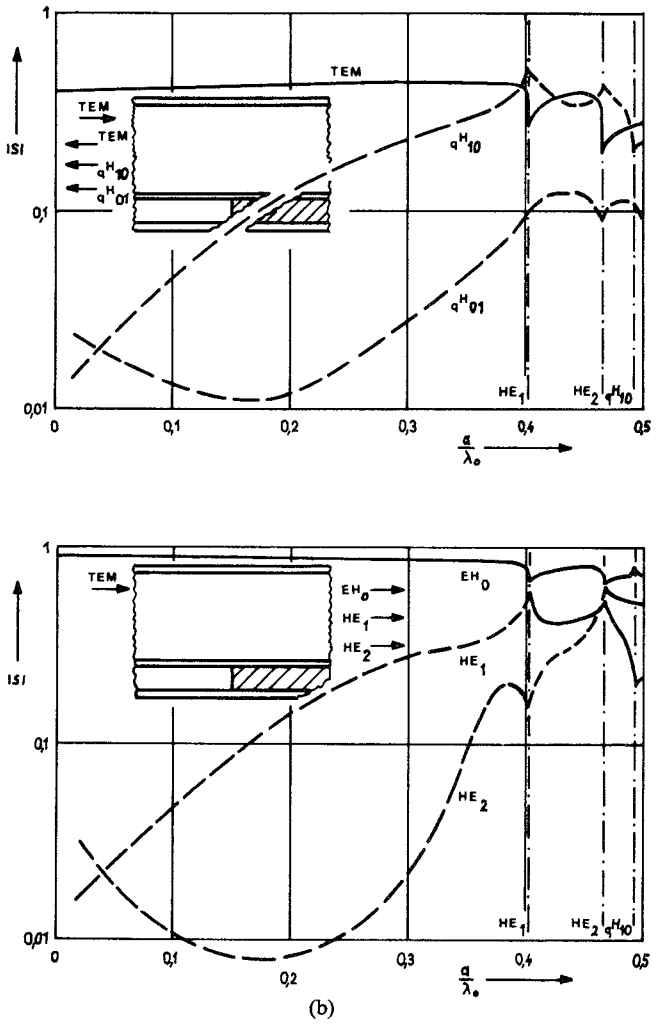

(b)

Fig. 4. Scattering coefficients of the first three modes of the step from the homogeneous shielded transmission line to the microstrip line (example ② of Fig. 1(b)) according to (19). (a) Reflection coefficients on the homogeneous shielded transmission line if a TEM wave is incident. qH_{10} is quasi-H_{10}-mode (quasi-TE_{10}-mode) (the field is equivalent to a TE_{10}-mode if the inner conductor vanishes), etc., (--- scattering coefficient below the corresponding cutoff frequency). (b) Transmission coefficients on the microstrip if a TEM wave is incident on the homogeneous line.

percent. For the computations presented here N was chosen to be ten.

The scattering matrix (19) of the steps for the three examples of Fig. 1(b) has been calculated. In Fig. 4 the amount of the first scattering coefficients, for example (2) of Fig. 1(b), is shown if a TEM wave is incident at the homogeneous transmission line. As expected the TEM wave transmits a large amount of its energy to the first hybrid mode (fundamental mode) on the microstrip, the other part is reflected (TEM wave). Beyond their cutoff frequency the higher order hybrid modes take over a large part of the energy. The cutoff frequency of the first higher order hybrid mode limits the practically significant range of application. If only the fundamental mode propagates, approximately the classical transmission line theory can be used, e.g., in the form of Carlin's network model [15]. This approximate theory is, however, only available if the effective dielectric constant as well as the characteristic impedance are known.

In Fig. 5 the characteristic impedance curves according to (20) of the microstrip examples of Fig. 1(b) are shown. There are also indicated the cutoff frequencies a/λ_{0c} of the first higher order mode of the examples (1) and (2) (that of example (3) lies beyond $a/\lambda_0 = 0{,}4$). For thick strips (example (1)), and for low frequencies and frequencies in the near of the cutoff frequency, we obtain an increasing function as it is indicated in [3]–[8] for thin strips and for the whole frequency range, but for mean frequencies the characteristic impedance decreases as indicated by Denlinger [2] also for the whole frequency range. The dotted line shows values using his definition for thick strips (example (1)), thus showing its limitation. For thin strips (example (2) and especially (3)) we find good agreement between his results and ours.

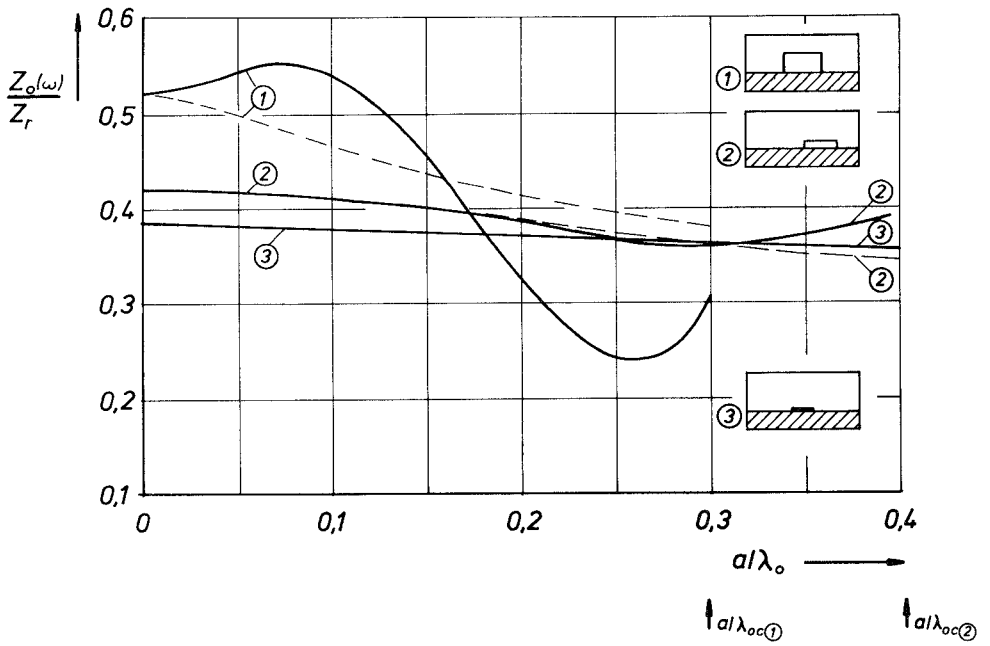

Fig. 5. Characteristic impedance $Z_0(\omega)/Z_r$ versus a/λ_0 of the microstrip lines of Fig. 1(b) according to (20). Z_r is the characteristic impedance of the rectangular transmission line (c.f. e.g., [9], [10]). --- characteristic impedance according to Denlinger's expression [2]: $Z_0(\omega)/Z_r = k_0/k_z$. (The curve ③ is nearly identical with the values of the above expression so that the dotted line is not shown. The values of (20) and of Denlinger's expression are so normalized that they are identical for $a/\lambda_0 = 0$.) ① $Z_r = 50\ \Omega$; ② $Z_r = 57.5\ \Omega$; ③ $Z_r = 65\ \Omega$.

APPENDIX I

The transition matrixes K_{III}^{II} and K_{II}^{I} are given by

$$\begin{bmatrix} U_h^{III} \\ U_e^{III} \\ I_h^{III} \\ I_e^{III} \end{bmatrix}_{y=y_u^{III}} = \begin{bmatrix} \frac{2}{a}K_c^t & -\frac{pu}{q}\frac{2}{a}K_c^t & 0 & 0 \\ 0 & \frac{1-u}{q}\frac{2}{a}K_s^t & 0 & 0 \\ 0 & 0 & (1-u)(K_c^tK_c)^{-1}K_c^t\frac{\tilde{g}}{2} & 0 \\ 0 & 0 & -pu(K_s^tK_s)^{-1}K_s^t\frac{\tilde{g}}{2} & q(K_s^tK_s)^{-1}K_s^t\frac{\tilde{g}}{2} \end{bmatrix} \begin{bmatrix} U_h^{II} \\ U_e^{II} \\ I_h^{II} \\ I_e^{II} \end{bmatrix}_{y=y_l^{II}} \tag{A1}$$

and

$$\begin{bmatrix} U_h^{II} \\ U_e^{II} \\ I_h^{II} \\ I_e^{II} \end{bmatrix}_{y=y_u^{II}} = \begin{bmatrix} (K_cK_c^t)^{-1}K_c\frac{a}{2} & 0 & 0 & 0 \\ 0 & (K_sK_s^t)^{-1}K_s\frac{a}{2} & 0 & 0 \\ 0 & 0 & \frac{2}{\tilde{g}}K_c & 0 \\ 0 & 0 & 0 & \frac{2}{\tilde{g}}K_s \end{bmatrix} \begin{bmatrix} U_h^{I} \\ U_e^{I} \\ I_h^{I} \\ I_e^{I} \end{bmatrix}_{y=y_l^{I}} \tag{A2}$$

with the abbreviations:

$$p = \sqrt{\frac{\epsilon_{eff}}{\epsilon_0\epsilon_r}} \qquad q = \frac{1}{\epsilon_r} \qquad u = \frac{\epsilon_0\epsilon_r - \epsilon_0}{\epsilon_0\epsilon_r - \epsilon_{eff}}$$

and

$$(K_c)_{ij}=\begin{cases}\displaystyle\int_0^g \frac{\cos\frac{i\pi x}{g}}{\sqrt{1+\delta_{0i}}}\,\frac{\cos\frac{j\pi x}{a}}{\sqrt{1+\delta_{0j}}}\,dx, & i<N^{IIa}\\ \displaystyle\int_{g+c}^a \frac{\cos\frac{\nu\pi(x-g-c)}{a-g-c}}{\sqrt{1+\delta_{0\nu}}}\,\frac{\cos\frac{j\pi x}{a}}{\sqrt{1+\delta_{0j}}}\,dx, & i>N^{IIa},\ \nu=i-N^{IIa}-1\end{cases}. \tag{A3}$$

K_c^t is the transposed matrix, K_s corresponds to the terms in (A3) with sine instead of cosine. N^{IIa} is the number of eigenfunctions considered in the partial waveguide IIa, Fig. 2.

Appendix II

Eigenfunctions $T(x,y)$ for the rectangular transmission line:

H-modes:

$$T_h^{I}=\sum_{n=0}^{\infty} A_n \frac{\cos\frac{n\pi x}{a}}{\sqrt{1+\delta_{on}}}\cos\left[k_{yn}^{I}(y+d/2+h-b)\right]$$

$$T_h^{IIa}=\sum_{n=0}^{\infty} \frac{\cos\frac{n\pi x}{g}}{\sqrt{1+\delta_{on}}}\left[B_n^a\cos\left(k_{yn}^{IIa}y\right)+C_n^a\frac{\sin\left(k_{yn}^{IIa}y\right)}{k_{yn}^{IIa}}\right]$$

$$T_h^{IIb}=\sum_{n=b}^{\infty} \frac{\cos\frac{n\pi(x-g-c)}{a-g-c}}{\sqrt{1+\delta_{on}}}\cdot\left[B_n^b\cos\left(k_{yn}^{IIb}y\right)+C_n^b\frac{\sin\left(k_{yn}^{IIb}y\right)}{k_{yn}^{IIb}}\right]$$

$$T_h^{III}=\sum_{n=0}^{\infty} D_n\frac{\cos\frac{n\pi x}{a}}{\sqrt{1+\delta_{on}}}\cos\left[k_{yn}^{III}(y+d/2+h)\right]. \tag{A4}$$

E-modes:

$$T_e^{I}=\sum_{n=1}^{\infty} A_n\sin\frac{n\pi x}{a}\,\frac{\sin\left[k_{yn}^{I}(y+d/2+h-b)\right]}{k_{yn}^{I}}$$

$$T_e^{IIa}=\sum_{n=1}^{\infty}\sin\frac{n\pi x}{g}\left[B_n^a\frac{\sin\left(k_{yn}^{IIa}y\right)}{k_{yn}^{IIa}}+C_n^a\cos\left(k_{yn}^{IIa}y\right)\right]$$

$$T_e^{IIb}=\sum_{n=1}^{\infty}\sin\frac{n\pi(x-g-c)}{a-g-c}\cdot\left[B_n^b\frac{\sin\left(k_{yn}^{IIb}y\right)}{k_{yn}^{IIb}}+C_n^b\cos\left(k_{yn}^{IIb}y\right)\right]$$

$$T_e^{III}=\sum_{n=1}^{\infty} D_n\sin\frac{n\pi x}{a}\,\frac{\sin\left[k_{yn}^{III}(y+d/2+h)\right]}{k_{yn}^{III}}. \tag{A5}$$

TEM-modes:

$$T_e^{I}=\sum_{n=1}^{\infty} A_n\sin\frac{n\pi x}{a}\sinh\frac{n\pi(y+d/2+h-b)}{a}$$

$$T_e^{IIa}=I_1 x/g e^{-jk_z z}+\sum_{n=1}^{\infty}\sin\frac{n\pi x}{g}\cdot\left[B_n^a\sinh\frac{n\pi y}{g}+C_n^a\cosh\frac{n\pi y}{g}\right]$$

$$T_e^{IIb}=I_1\frac{a-x}{a-g-c}e^{-jk_z z}+\sum_{n=1}^{\infty}\sin\frac{n\pi(x-g-c)}{a-g-c}\cdot\left[B_n^b\sinh\frac{n\pi y}{a-g-c}+C_n^b\cosh\frac{n\pi y}{a-g-c}\right]$$

$$T_e^{III}=\sum_{n=1}^{\infty} D_n\sin\frac{n\pi x}{a}\sinh\frac{n\pi(y+d/2+h)}{a}. \tag{A6}$$

References

[1] B. Bianco, L. Panini, M. Parodi, and S. Ridella, "Some considerations about the frequency dependence of the characteristic impedance of uniform microstrips," *IEEE Trans. Microwave Theory Tech.*, vol. MTT-26, pp. 182–185, Mar. 1978.

[2] E. J. Denlinger, "A frequency dependent solution for microstrip transmission lines," *IEEE Trans. Microwave Theory Tech.*, vol. MTT-19, pp. 30–39, 1971.

[3] H. J. Schmitt and K. H. Sarges, "Wave propagation in microstrip," *Nachrichtentech. Z.*, vol. 24, pp. 260–264, 1971.

[4] M. K. Krage and G. I. Haddad, "Frequency-dependent characteristics of microstrip transmission lines," *IEEE Trans. Microwave Theory Tech.*, vol. MTT-20, pp. 678–688, 1972.

[5] G. Kowalski and R. Pregla, "Dispersion characteristics of single and coupled microstrips," *Arch. Elek. Ubertragung*, vol. 26, pp. 276–280, 1972.

[6] R. P. Owens, "Predicted frequency dependence of microstrip characteristic impedance using the planar-waveguide model," *Electron. Lett.*, vol. 12, no. 11, pp. 269–270, May 27, 1976.

[7] J. B. Knorr and A. Tufekcioglu, "Spectral-domain calculation of microstrip characteristic impedance," *IEEE Trans. Microwave Theory Tech.*, vol. MTT-23, pp. 725–728, Sept. 1975.

[8] R. H. Jansen, "High speed computation of single and coupled microstrip parameter including dispersion, high-order modes, loss and finite strip thickness," *IEEE Trans. Microwave Theory Tech.*, vol. MTT-26, pp. 75–81, Feb. 1978.

[9] W. Bräckelmann, "Wellentypen auf der Streifenleitung mit rechteckigem Schirm," *Arch. Elek. Übertragung*, vol. 21, pp. 641–648, 1976.

[10] W. S. Metcalf, "Characteristic impedance of rectangular transmission lines," *Proc. IEEE*, vol. 112, pp. 2033–2039, Nov. 1965.

[11] G. U. Paul, "Über den Wellenwiderstand der Mikrostreifenleitung," *Arch. Elek. Übertragung*, vol. 30, pp. 463–464, 1976.

[12] ——, "Berechnung des sprunghaften Übergangs vom Rechteck-

hohlleiter zur geschirmten Streifenleitung mit homogenem sowie inhomogenem Dielektrikum," Ph.D. dissertation, Univ. of Bremen, Germany, 1976.
[13] G. Kowalski and R. Pregla, "Dispersion characteristics of shielded microstrips with finite thickness," *Arch. Elek. Ubertragung*, vol. 25, pp. 193–196, 1971.
[14] R. Mittra and T. Itoh, "A new technique for the analysis of the dispersion characteristics of microstrip lines," *IEEE Trans. Microwave Theory Tech.*, vol. MTT-19, pp. 47–56, 1971.
[15] H. J. Carlin, "A simplified circuit model for microstrip," *IEEE Trans. Microwave Theory Tech.*, vol. MTT-21, pp. 589–591, Sept. 1973.

Analysis of an End Launcher for an *X*-Band Rectangular Waveguide

MANOHAR D. DESHPANDE, MEMBER, IEEE, B. N. DAS, AND GITINDRA S. SANYAL

***Abstract*—The analysis of an end-laucher type, coaxial-to-rectangular waveguide transition, exciting dominant TE_{01} mode in *X*-band rectangular waveguide is presented. Expressions for the real and imaginary parts of the input impedance seen by the coaxial line are derived for the general case of an offset launcher using self-reaction of an assumed current over the loop. The dimensions of the combined electric and magnetic loops having low input VSWR in the coaxial line are determined. There is satisfactory agreement between theoretical and experimental results.**

I. Introduction

For the excitation of a two-dimensional array of rectangular waveguide radiators it is found convenient [1], [2] to use a colinear end-launcher transition from coaxial line-to-rectangular waveguide. Investigations on these types of transitions have been carried out by a number of workers. Wheeler [3] has empirically investigated the design of such a transition by matching the waveguide-to-coaxial line with the help of two step ridge transformers. Dix [4] also established a theoretical design procedure for the transition with a mixed four-section impedance transformer consisting of two ridged steps within the waveguide, one TEM section in the coaxial line, and a hybrid section where the coaxial center-conductor extends into the guide. A theoretical analysis for the design of a transition consisting of an L-shaped concentric loop without any additional impedance transformer has been presented by Das and Sanyal [5]. In their design, the dimensions of the L-shaped loop were selected in such a way that the real part of the input impedance seen by the coaxial line was equal to characteristic impedance of the coaxial line. The input reactance cancellation was achieved by a trial and error method. The bandwidth of the transition was very narrow. The maximum input VSWR of the transition was found to be 1.4 over the frequency range 9.2–9.5 GHz (300 MHz). The bandwidth of this type of transition can be more accurately determined, and a method of its improvement can be found if the explicit expressions for both real and imaginary parts of the input impedance seen by the coaxial line in terms of loop dimensions L_1, a', and b' (Fig. 1) are known.

In this paper, a more general analysis applicable to concentric as well as offset launcher in the form of an L-shaped loop placed in a dominant TE_{01}-mode rectangular waveguide is presented. The expressions for both the real and imaginary parts of input impedance seen by the coaxial line are derived from the self-reaction of an assumed current over the probe. The expression for the real part of input impedance is then used to find the loop dimensions L_1, a', and b' which give the real part of input impedance to be equal or close to characteristic impedance of the coaxial line over a range of frequencies. The variation of input reactance for these loop dimensions is computed as a function of frequency. From the variation of input impedance, the loop dimensions L_1, a', and b' which give low input VSWR in the coaxial line over a range of frequencies are determined. Theoretical and experimental results for input VSWR are compared for a transition with $L_1 = 1.4$ cm, $a' = 0.4$ cm, $b' = 1.15$ cm, and the probe diameter $2R = 0.2$ cm.

II. Analysis

Fig. 1(a) shows an L-shaped loop placed in a dominant TE_{01}-mode rectangular waveguide and driven from a generator through a coaxial line. The input impedance seen by the coaxial line driving the L-shaped loop is obtained from a stationary formula [6]:

$$Z_{\text{in}}|_c = -\int_v \frac{\vec{E}\cdot\vec{J}}{I_{\text{in}}^2}\,dv \tag{1}$$

where $\vec{E}$ is the electric field inside the guide due to

Manuscript received June 14, 1978; revised October 18, 1978.
The authors are with the Department of Electronics and Electrical Communications Engineering, Indian Institute of Technology, Kharagpur 721302, India.

0018-9480/79/0800-0731$00.75 ©1979 IEEE